Source Process of the 2007 Niigata-ken Chuetsu-oki Earthquake
Derived from Near-fault Strong Motion Data

National Research Institute for Earth Science and Disaster Prevention

The 2007 Niigata-ken Chuetsu-oki earthquake occurred on July 16th, 2007, 10:13 JST (37.557N, 138.608E, 17 km depth; Japan Meteorological Agency). We performed a multi-time window linear waveform inversion analysis (Hartzell and Heaton, 1983) to estimate the rupture process from the near fault strong motion data of K-NET, KiK-net, and others.

Fault Model and Parameterization

Open circles in Fig. 1 are aftershock distribution within 24 hours of the mainshock located by manual picking of Hi-net data. Fault mechanisms are estimated by the distribution of the polarity for the P-wave first motion by Hi-net (left) and by the moment tensor analysis of F-net data (right).

The fault plane for the mainshock has not been clearly determined yet from the aftershock distribution, so that we performed two waveform inversions for north-west dipping fault (Model A) and south-east dipping fault (Model B). Their strike, dip and rake (as the center of the rake angle variation constraint) are set to those of the moment tensor solutions by F-net. The former is N215E, 49, 80 degrees, and the latter is N49E, 42, 101 degrees for strike, dip, rake angles, respectively. The hypocenter determined by hypoDD using Hi-net data (Yukutake et al., 2007) was 37.5397N, 138.6091E, and 7.417 km depth. For waveform inversion, we assumed a rupture starting point at the same epicenter and 8 km depth.

We assumed a fault plane model of 30 km length by 24 km width to cover aftershock distribution within 24 hours after the mainshock. In the multi-time window linear waveform inversion procedure, the moment-release distribution is discretized in both space and time. Discretization in space is done by dividing the model fault planes into 180 subfaults, each 2 km× 2 km. We assumed six smoothed ramp functions with 1.0 sec duration separated by 0.5 sec to represent slip velocity time function on each subfault.

Theoretical Green's functions were calculated by the discrete wavenumber method (Bouchon, 1981) and the R/T matrix method (Kennett, 1983) with the different stratified medium for each station based on the velocity structure including the information form the reflection survey and borehole logging data. Convolution of moving dislocation was introduced to represent the rupture propagation in an each subfault (Sekiguchi et al., 2002).

Waveform Data

We used strong motion data of 14 stations shown in Fig. 1 from K-NET, KiK-net

(downhole), F-net, JMA (JMACB6), and Niigata prefecture (L65039). The observed acceleration records were integrated into velocity except of F-net velocity data recorded by VSE-355G2, and bandpass filtered between 0.1 and 1.0 Hz. We inverted 14 s of the S-wave portion from 1 s before the S-wave arrivals.

Waveform Inversion

We solved least-squared equation to obtain slip amount of each time window on each subfault to minimize squared residual of the waveform fitting between observed and synthetic waveforms. To reduce instability or excessive complexity, smoothing constraint is introduced to reduce differences among slips close in space and in time. Non-negative constraints (Lawson and Hanson, 1974) to limit the rake-angle variation are also adopted. The rake angles were allowed to vary within plus-minus 45 degree centered at 101 degree for north-west dipping fault and 80 degree for south-east dipping fault, which are rake angles of the moment tensor solutions by F-net. We performed many inversions changing the rupture velocity of the first time windows and the smoothing strength. Appropriate values for the smoothing strength and the rupture velocity were selected based on ABIC (Akaike's Bayesian Information Criterion; Akaike, 1980) and the residual of the waveform fitting, respectively.

Result

Fig. 2 show slip distributions and Fig. 3 displays comparison between observed and synthetic velocity waveforms.

Regarding Model A (north-west dipping fault plane), estimation of the total seismic moment was 1.42 x 10^{19} Nm which corresponds to Mw = 6.7. We obtained large slip in the south-west deeper part of the rupture starting point, which is close to Kashiwazaki-city. The second or third velocity pulses of observed velocity waveforms seem to be composed of slip from the asperity.

Regarding Model B (south-east dipping fault plane), estimation of the total seismic moment was 1.62 x 10^{19} Nm which corresponds to Mw = 6.7. We obtained large slip in the southwest shallower part of the rupture starting point, which is also close to Kashiwazaki-city.

In both models, we found small slip near the rupture starting point, and largest slip at about ten kilometer in the south-west of the rupture starting point with the maximum slip of 2.3 and 2.5 m for Models A and B, respectively. The difference of the residual between observed and synthetic waveforms for both models is not significant, therefore it is difficult to conclude which fault plane is appropriate to explain. The estimated large-slip regions in the inverted source models with the Models A and B are located near the cross point of the two fault plane models, which should have similar radiation pattern. This situation may be one of

the reasons why judgment of the fault plane orientation is such difficult. We need careful examinations not only strong motion data but also geodetic data to further explore the fault orientation and the source process of this earthquake.

Notes: This result is preliminary and will make a change.

(*Aoi, S.(aoi@bosai.go.jp), **H. Sekiguchi, *N. Morikawa, *T. Kunugi, and ***M. Shirasaka)
* National Research Institute for Earth Science and Disaster Prevention
** National Institute of Advanced Industrial Science and Technology
*** Japan Meteorological Agency

References

Akaike, H. (1980), Likelihood and the Bayes procedure, in Baysesian statics, edited by J. M. Bernardo, M. H. DeGroot and A. F. M. Smith, University Press, Valencia, Spain.

Bouchon, M. (1981), A simple method to calculate Green's function for elastic layered media, Bull. Seism. Soc. Am., 71, 959-971.

F-net, www.fnet.bosai.go.jp/freesia/index.html

Hartzell, S. H. and T. H. Heaton (1983), Inversion of strong ground motion and teleseismic waveform data for the fault rupture history of the 1979 Imperial Valley, California, earthquake, Bull. Seism. Soc. Am., 73, 1553-1583.

Hi-net, www.hinet.bosai.go.jp/ (in Japanese).

Kennett, B. L. and N. J. Kerry (1979), Seismic waves in a stratified half space, Geophys. J. R. astr. Soc., 57, 557-583.

Lawson, C. L., and R. J. Hanson (1974). Solving Least Squares Problems, Prentice-Hall, Inc., New Jersey, 340 pp.

Sekiguchi, H., K. Irikura, and T. Iwata. (2002). Source inversion for estimating continuous slip distribution on the fault, --- Introduction of Green's functions convolved with a correction function to give moving dislocation effects in subfaults ---, Geophys. J. Int., 150, 377-391, 2002.

Yukutake, Y., T. Takeda, K. Obara (2007), Spatial distribution of aftershocks in the region of Niigata Tyuetsu-oki Earthquake in 2007, by waveform correlation analysis, fall meeting of Seism. Soc. Japan (in Japanese).

Wessel, P., and W. H. F. Smith (1995). New version of the Generic Mapping Tools released, EOS Trans. AGU 76, 329.
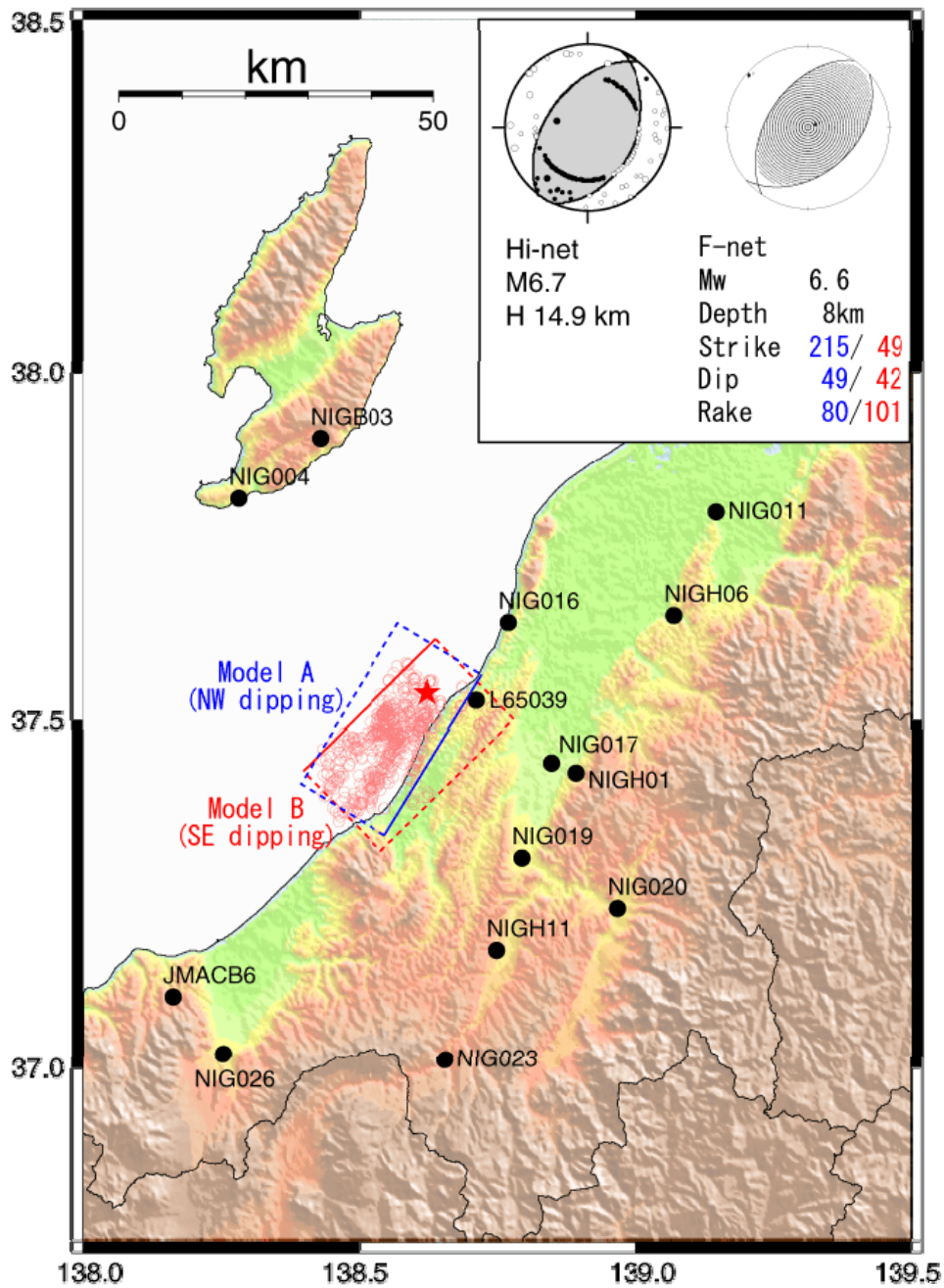
Fig. 1: Distribution of the observation stations used for the inversion analysis. Two rectangles show the projection of the assumed fault planes. Red star indicates the rupture starting point. Open circles are aftershock distribution within 24 hours after the mainshock located by manual picking of Hi-net data. Fault mechanisms are estimated by the distribution of the polarity for the P-wave first motion by Hi-net (left) and by the moment tensor analysis of F-net data (right).
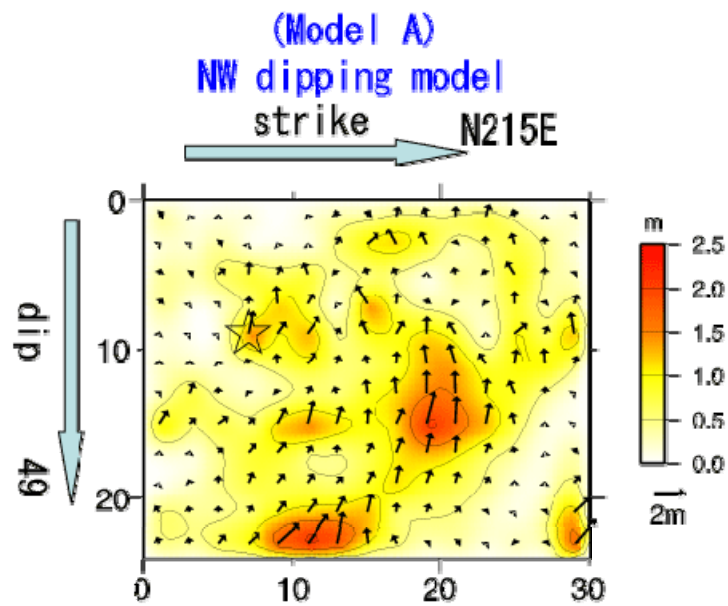
Fig. 2A: Estimated total slip distribution (north-west dipping fault; Model A). Star indicates the rupture starting point. Arrows show the amplitudes and directions of slip.
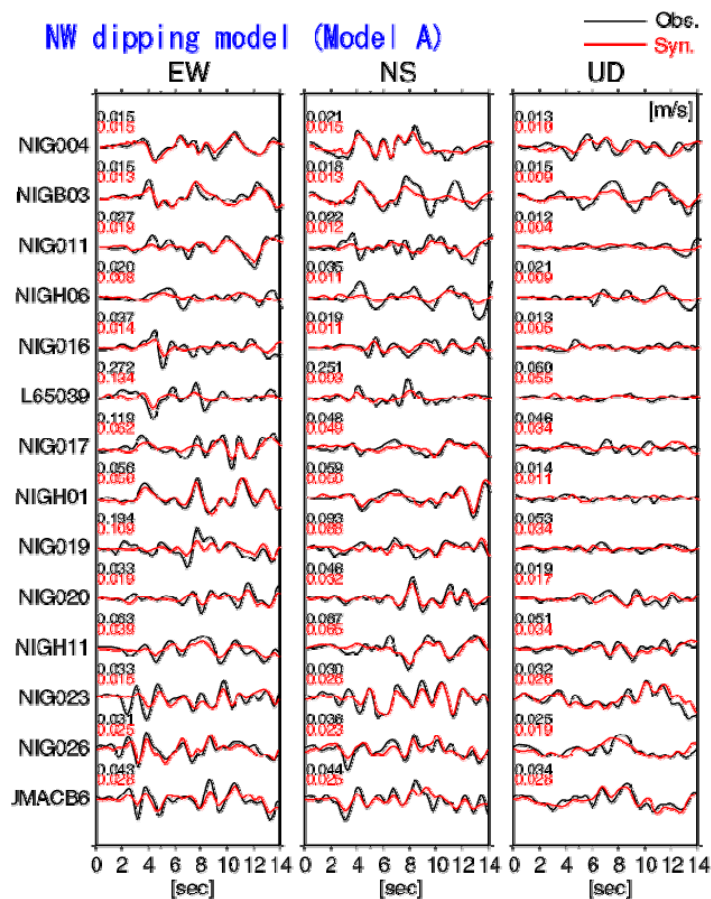

Fig. 3A: Comparison between observed (black) and synthetic (red) velocity waveforms (north-west dipping fault; Model A). The maximum values of each component are given to the upper-left of each trace in m/s.
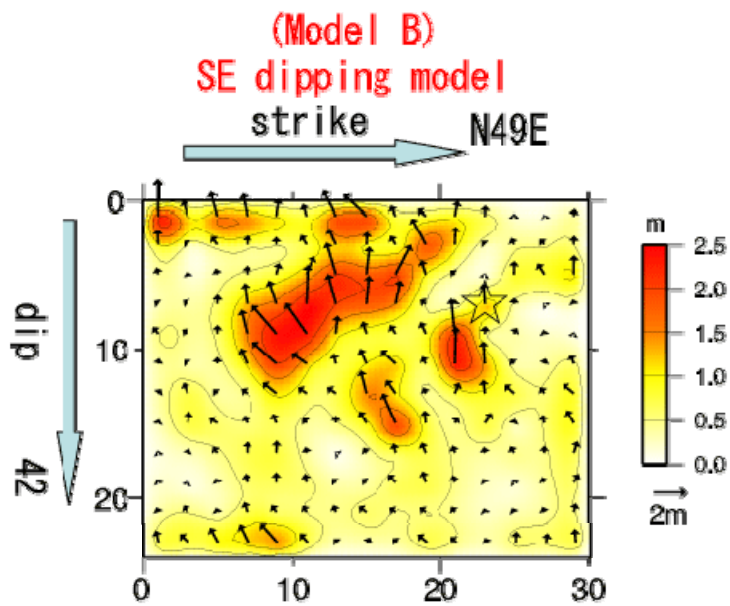
Fig. 2B: Estimated total slip distribution (south-east dipping fault; Model B) Star indicates the rupture starting point. Arrows show the amplitudes and directions of slip.
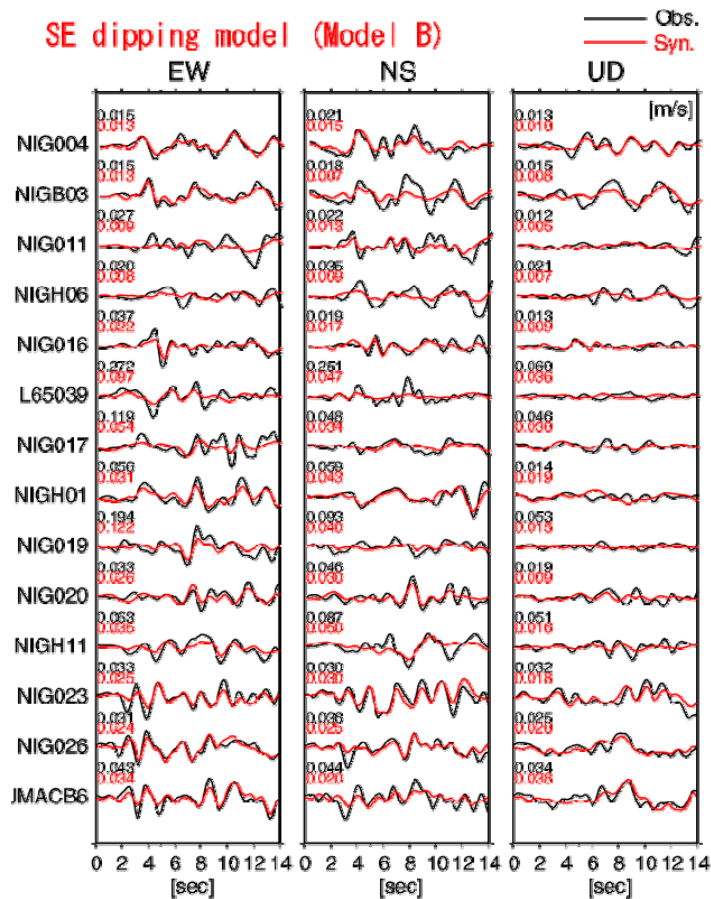

Fig. 3B: Comparison between observed (black) and synthetic (red) velocity waveforms (south-east dipping fault; Model B). The maximum values of each component are given to the upper-left of each trace in m/s.
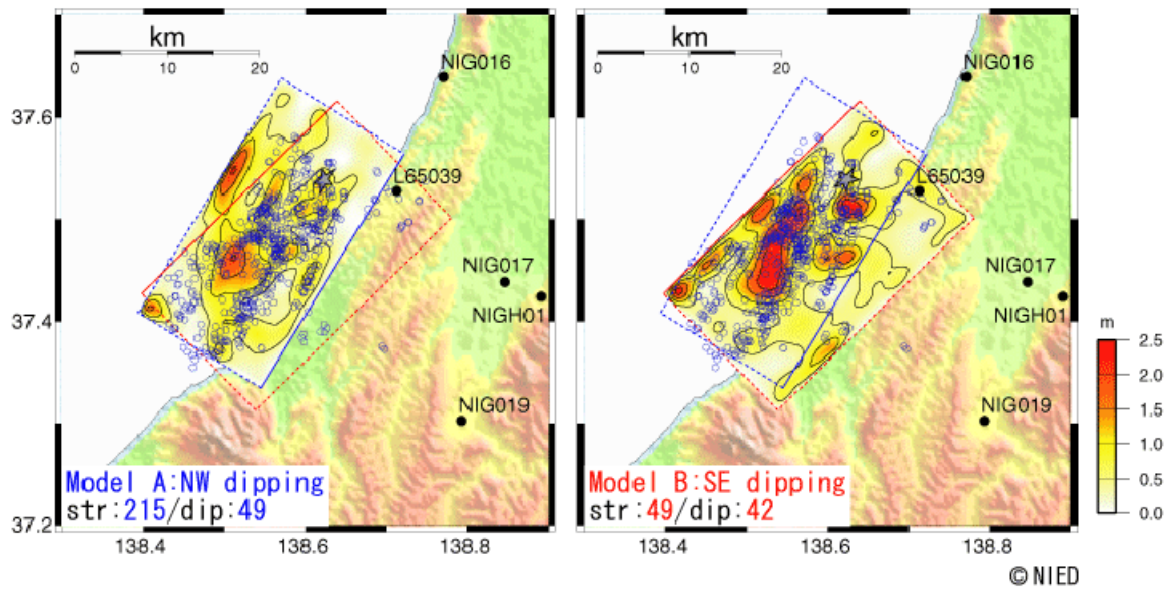
Fig. 4: The projection of the inverted slip distribution. Left panel is Model A (north-west dipping fault), and right panel is Model B (south-east dipping fault). Blue circles are aftershock distributionlocations estimated by hypoDD using Hi-net data (Yukutake et al., 2007). The large slip area falls on to the area with relatively sparse aftershock distribution.